Brain and Spine 2 (2022) 100859

Contents lists available at ScienceDirect

Brain and Spine

journal homepage: www.journals.elsevier.com/brain-and-spine

In vivo imaging in experimental spinal cord injury – Techniques and trends

Vanessa Hubertus [a], Lea Meyer [a], Laurens Roolfs [a], Lilly Waldmann [a], Melina Nieminen-Kelhä [a], Michael G. Fehlings [b,1], Peter Vajkoczy [a,*,1]

[a] *Charité – Universitätsmedizin Berlin, Corporate Member of Freie Universität Berlin, Humboldt-Universität zu Berlin, And Berlin Institute of Health, Department of Neurosurgery, Berlin, Germany*
[b] *Toronto Western Hospital, Department of Neurosurgery and Spinal Program, University Health Network, Toronto, Canada*

ARTICLE INFO

Keywords:
Spinal cord injury
Spinal cord regeneration
In vivo studies
Animal studies
Modern imaging
In vivo imaging

ABSTRACT

Introduction: Traumatic Spinal Cord Injury (SCI) is one of the leading causes of disability in the world. Treatment is limited to supportive care and no curative therapy exists. Experimental research to understand the complex pathophysiology and potential mediators of spinal cord regeneration is essential to develop innovative translational therapies. A multitude of experimental imaging methods to monitor spinal cord regeneration *in vivo* have developed over the last years. However, little literature exists to deal with advanced imaging methods specifically available in SCI research.

Research Question: This systematic literature review examines the current standards in experimental imaging in SCI allowing for *in vivo* imaging of spinal cord regeneration on a neuronal, vascular, and cellular basis.

Material and Methods: Articles were included meeting the following criteria: experimental research, original studies, rodent subjects, and intravital imaging. Reviewed in detail are microstructural and functional Magnetic Resonance Imaging, Micro-Computed Tomography, Laser Speckle Imaging, Very High Resolution Ultrasound, and *in vivo* microscopy techniques.

Results: Following the PRISMA guidelines for systematic reviews, 689 articles were identified for review, of which 492 were sorted out after screening and an additional 104 after detailed review. For qualitative synthesis 93 articles were included in this publication.

Discussion and Conclusion: With this study we give an up-to-date overview about modern experimental imaging techniques with the potential to advance the knowledge on spinal cord regeneration following SCI. A thorough knowledge of the strengths and limitations of the reviewed techniques will help to optimally exploit our current experimental armamentarium in the field.

1. Introduction

Traumatic spinal cord injury (SCI) is one of the world's leading causes of disability (Singh et al., 2014; Cripps et al., 2010; Majdan et al., 2017; Badhiwala et al., 2018). No curative therapy exists, and treatment is limited to supportive care. In the past decades, experimental research brought tremendous progress to the basic knowledge of the complex pathophysiology underlying SCI, as well as to the endogenous regenerative responses of the spinal cord. With advancing knowledge, research is shifting from the general characterization of SCI pathophysiology to the potential amelioration of spinal cord regeneration via targeting endogenous repair mechanisms (Monje, 2021). Experimental studies using longitudinal *in vivo* imaging play a significant role in the characterization of potential targets for advancing spinal cord regeneration.

Experimental imaging of CNS pathologies has evolved widely over the past decades. In comparison to classical histological tissue analysis, longitudinal *in vivo* imaging allows for an increasingly accurate morphological and functional tissue analysis in the same subject at different time points. With high dynamics and a high spatial resolution, longitudinal *in vivo* imaging can be performed non-invasively and therefore repeatedly. This does not only increase comparability, but also reduces the necessary group sizes in animal experimental research. In SCI, *in vivo* imaging evolved over the last years from the mere morphological assessment of trauma size and regeneration to the possibility of live tracking of spinal cord injury and regeneration on a neuronal, vascular, and even on a cellular level. These techniques allow

* **Corresponding author.** Charité - Universitätsmedizin Berlin, Department of Neurosurgery, Charitéplatz 1, 10117, Berlin, Germany.
E-mail address: peter.vajkoczy@charite.de (P. Vajkoczy).
[1] Equally contributing, shared senior authors.

https://doi.org/10.1016/j.bas.2021.100859
Received 18 October 2021; Received in revised form 15 December 2021; Accepted 22 December 2021
Available online 29 December 2021

furthermore for real-time tracking and longitudinal follow-up of the regenerative capacities of experimental therapies.

However, little literature exists to deal with the multitude of advanced experimental imaging methods specifically available in SCI research, and their capacities to enhance the understanding of spinal cord regeneration.

2. Material and methods

2.1. Approach to the systematic literature review

We performed a systematic review of the literature. The Medline databases Pubmed and Pubmed central, as well as CINAHL, Embase, Google Scholar and Science Direct were searched. The main search terms included Spinal Cord Injury, Intravital Imaging, Intravital Microscopy, Magnetic Resonance Imaging (MRI), Ultrasound, Photoacoustic Imaging, Laser Speckle Imaging, and Micro-Computed Tomography (μCT), in combination with Spinal Cord Injury and rodent subjects. The search included no time limit. Articles in English were included, meeting the following criteria: experimental research, original studies, rodent subjects, intravital imaging including MRI, μCT, Intravital Microscopy, Laser Speckle Imaging or Ultrasound techniques. The systematic literature search was conducted independently by four researchers from March 2020–November 2021. Data analysis was conducted according to the PRISMA (Preferred Reporting Items for Systematic Reviews and Meta-Analyses) guidelines. Obtained for review were 689 articles, of which 492 were sorted out after screening due to not meeting the inclusion criteria. An additional 104 articles were excluded due to not meeting the inclusion criteria after full-text assessment for eligibility. For qualitative synthesis 93 articles were assessed in detail and included in this publication (Fig. 1: PRISMA flow chart).

2.2. Relevant experimental in vivo imaging methods according to the literature search

According to the systematic literature search and the inclusion of 93 articles for qualitative data synthesis, five main *in vivo* imaging techniques in use in experimental SCI research were identified: 1. Magnetic Resonance Imaging with functional (f)MRI and microstructural MRI, 2. Micro-CT (μCT), 3. Laser Speckle Contrast Imaging (LSCI), 4. Ultrasonography with Very High Resolution Ultrasound (VHRUS) and Photoacoustic Imaging (PA), and 5. Intravital Microscopy including Epifluorescence Videomicroscopy (IVM) and 2- or Multiphoton-Microscopy (TPEF). In the following, we discuss these topics in detail, including history, technical development, area of applications, strengths and weaknesses and potential outlook.

2.3. Illustrative examples of in vivo imaging

In Figs. 2–4, we display exemplary images of *in vivo* imaging methods

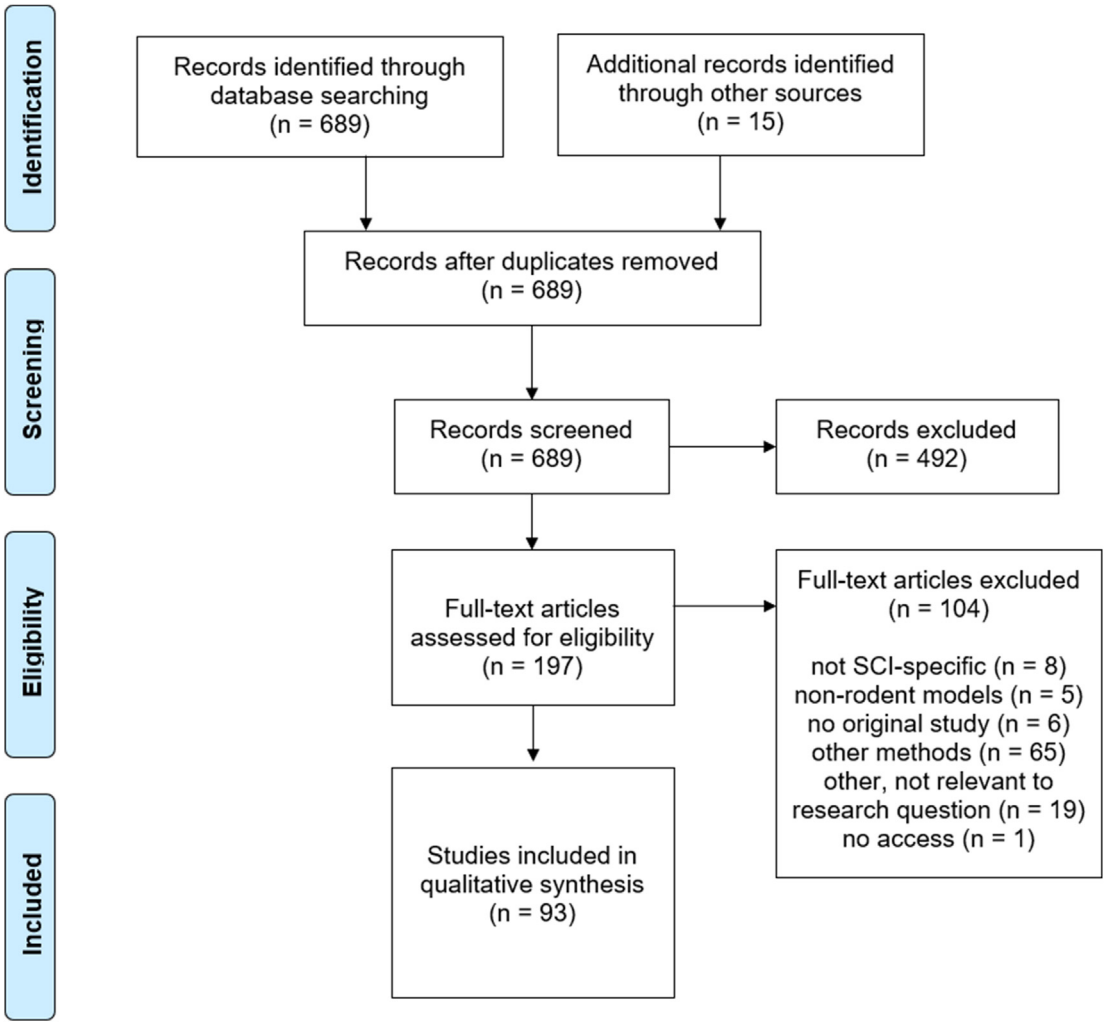

Fig. 1. Flow Chart of the conducted literature review and the systematic synthesis according to the PRISMA guidelines for systematic reviews and meta-analyses. (PRISMA – Preferred Reporting Items for Systematic Reviews and Meta-Analyses).

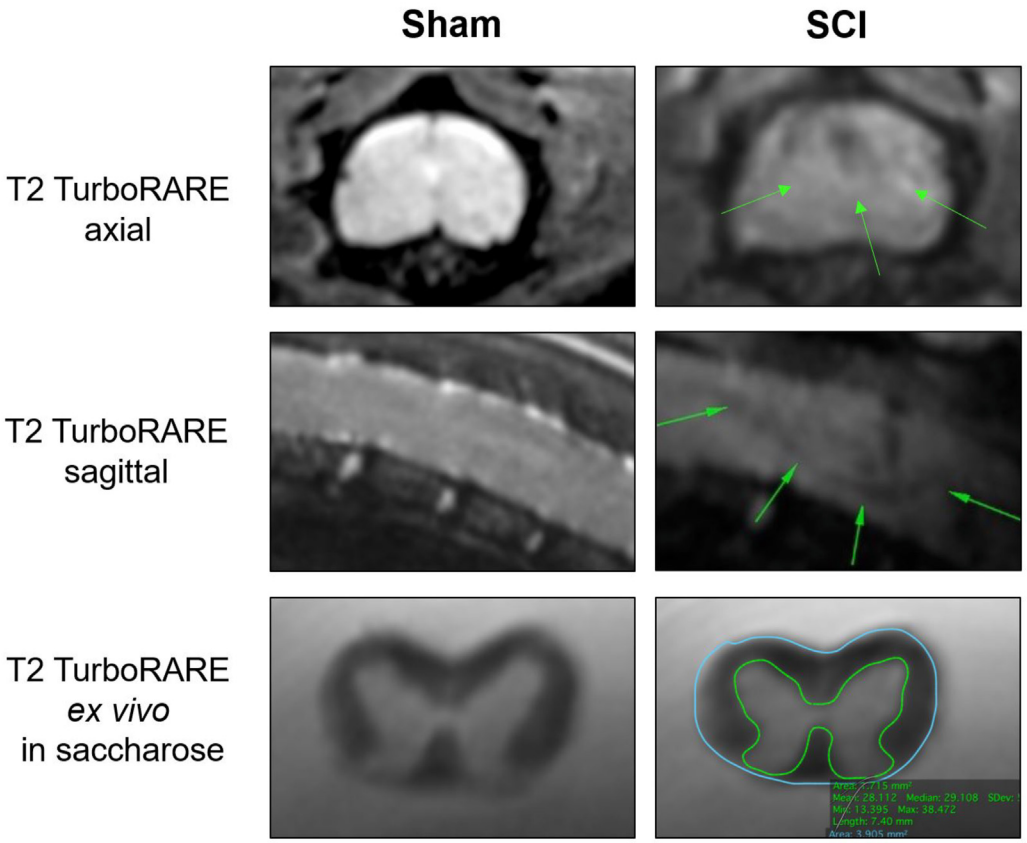

Fig. 2. *In vivo* T2 TurboRARE 7 T Magnetic Resonance Imaging in mice with Sham-injury and SCI for axial and sagittal imaging of the spinal cord (spinal cord swelling after SCI, green arrows). *Ex vivo* MRI (spinal cord in saccharose) following sacrifice is also possible with exact volumetry of grey and white matter as well as injury volumetry (in blue/green, right). (For interpretation of the references to color in this figure legend, the reader is referred to the Web version of this article.)

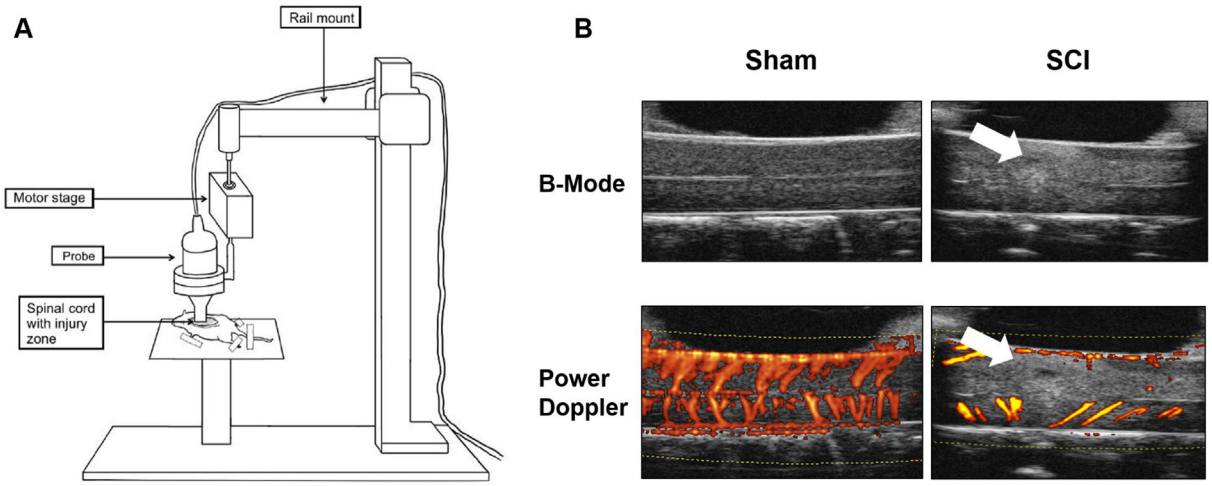

Fig. 3. **A** Technical Setting of *in vivo* Very High Resolution Ultrasound (VHRUS) in a murine model of experimental SCI. **B** Example of VHRUS of the intact (Sham) and injured (SCI) murine spinal cord in B-mode and Power Doppler mode for structural, functional and volumetrical analysis of SCI. The white arrows show structural alterations in a specimen with SCI. The images of VHRUS in B-Mode and Power Doppler Mode are printed with the permission of Michael G. Fehlings and Anna Badner.

performed at our institutions in murine specimens (C57BL/6J) with SCI or sham injury. The illustrative images were produced as by-products during the performance of experimental SCI studies conducted at our local institutions and were not previously published. All animal procedures were approved by the local governmental institutions (G0314/17). A continuous and close monitoring protocol was followed, and potent pain medication was applied as described in detail before (Soubeyrand et al., 2014a; Figley et al., 2014; Forgione et al., 2017). For SCI induction, the *Clip Compression Contusion Injury* model was used and for sham injury a two-level laminectomy without SCI was performed at the thoracic level (T6/7 or T10/11) (Joshi and Fehlings, 2002). For imaging procedures, volatile anesthesia (isoflurane; for magnetic resonance

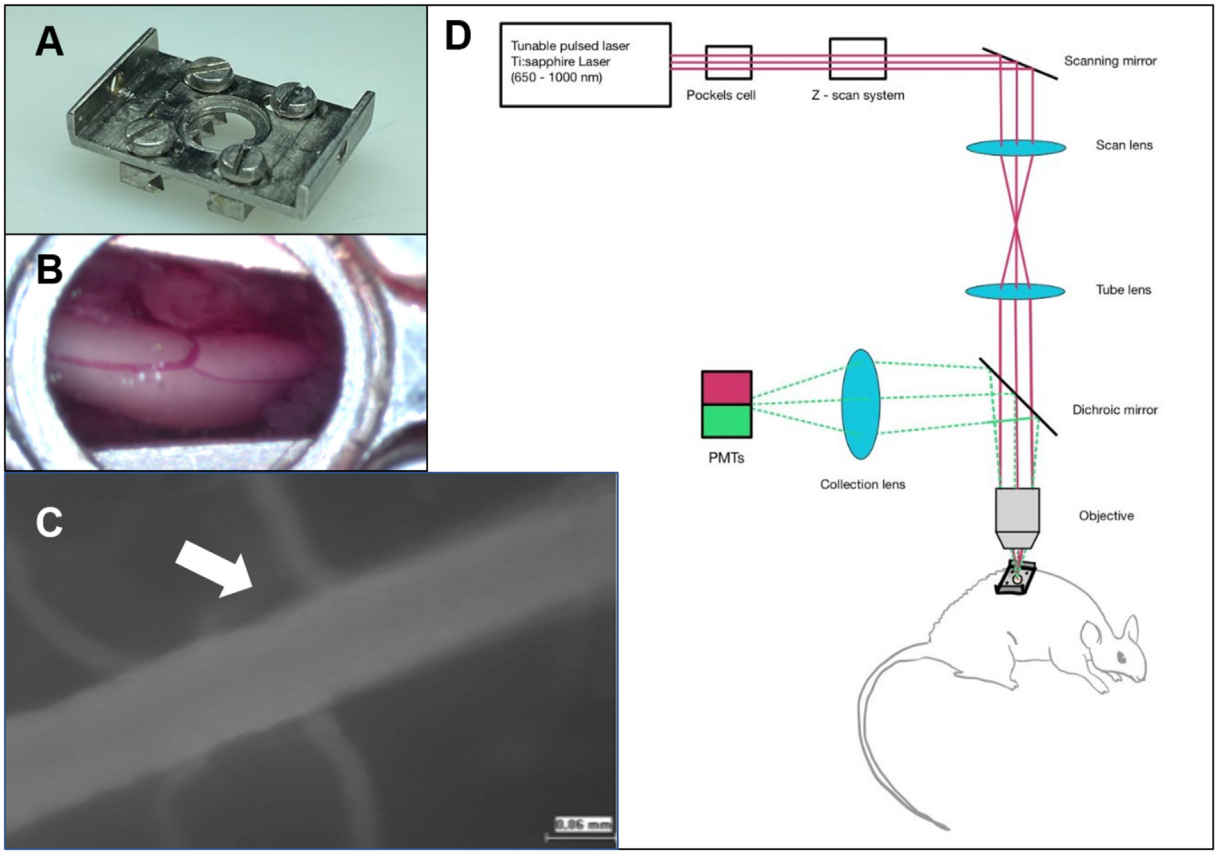

Fig. 4. Experimental setup of *in vivo* microscopy of the spinal cord via implanted spinal window chamber, adapted by Farrar et al. (**A** + **B**) *In vivo* video-epifluorescence microscopy via the implanted spinal window chamber at 7 days post implantation in a healthy specimen, with the arrow showing intact spinal cord vessels (**C**). Schematic setup of TPEF (Two-photon excitation fluorescence microscopy) in a murine model of experimental SCI using the spinal window chamber for longitudinal *in vivo* imaging (**D**).

imaging, MRI) or intravenous anesthesia (Ketamine, Xylazine; for Epi-fluorescence videomicroscopy and very high resolution ultrasound, VHRUS) was used. MRI was performed using a 7 T small-animal MRI scanner (7 T PharmaScan 70/20USR, Bruker corp.). For VHRUS, the VEVO 770 (FUJIFILM VisualSonics) ultrasound system was used (Soubeyrand et al., 2014a; Badner et al., 2016). For longitudinal *in vivo* microscopy, an implanted spinal window chamber adapted from Farrar et al. was implanted at the thoracic level following SCI or sham injury (Th10/11) and epifluorescence videomicroscopy was performed in the spinal cord as described before in the brain (Farrar et al., 2012; Vajkoczy et al., 1999; Uhl et al., 2018).

3. Theory

With this study we aim to comprehensively review experimental setups using *in vivo* imaging of different kind in SCI, to give an up-to-date overview to experimental researchers dealing with spinal cord regeneration and repair following SCI. In the following sections, we will review *in vivo* imaging techniques used in modern experimental settings to analyze SCI and spinal cord regeneration in detail.

4. Results

4.1. Structural and functional magnetic resonance imaging (MRI/fMRI)

4.1.1 History: Magnetic resonance imaging (MRI) and its derived techniques are the oldest of the imaging techniques discussed, with the underlying methods originating between the 1980s and early 2000s (Falconer et al., 1994; Basser et al., 1994; Malisza and Stroman, 2002; Ford et al., 1994; Ramu et al., 2006). The clinical use of MRI predates its use in animal experimental research. MRI as a tool to image experimental SCI in rodents was first established by Hackney et al., in 1986 (Ford et al., 1994). Falconer et al. in 1994 were the first to perform a longitudinal *in vivo* imaging study to quantify SCI pathology using MRI by constructing 3D-volume rendered images (Falconer et al., 1994). Within the first 5–10 years following the establishment of MRI in experimental SCI, the additional use of diffusion tensor imaging (DTI) appeared, though largely applied *ex vivo* (Cohen et al., 2009; Patel et al., 2016). Since 2002, functional MRI (fMRI) is established in experimental SCI, with its first application in the cervical spine in 2006 (Malisza and Stroman, 2002). Since the beginning of its use in animal experiments, MRI quality improved from 1,4 T to about 7–9 T, while in certain cases even ultra-high field resolution MR imaging is available at 16,4 T (Ford et al., 1994; Schwartz and Hackney, 2003; Brennan et al., 2013).

4.1.2 Technical: MRI scanners used for experimental imaging are not notably different to those used in the clinical setting, though with smaller bore sizes (30–90 cm) and an appropriately smaller surface coil. For improving image quality during *in vivo* imaging, implanted coils appeared at the time, but were abandoned later for their invasiveness with the technical evolvement of modern MRI scanners (Ford et al., 1994; Sundberg et al., 2010). Modern experimental MRI scanners can monitor breathing, and use respiratory and cardiac gating to reduce imaging artifacts produced by movement (Ford et al., 1994; Sundberg et al., 2010). At the beginning mostly T1 weighted imaging with or without contrast-enhancing and T2 or Rapid Acquisition with Relaxation Enhancement (RARE) sequences were used (Malisza and Stroman, 2002; Song et al., 2018; Sundberg et al., 2011). During the technical evolvement, Diffusion Tensor Imaging (DTI) became predominant, using

computer assistance to reconstruct axonal bundles on the diffusion of present water molecules in the tissue (Basser et al., 1994; Soares et al., 2013). Functional MRI (fMRI) uses Blood Oxygen Level Dependent (BOLD) contrast changes to detect active regions containing ascending and descending sensorimotor pathways in resting state or upon stimulation (Malisza and Stroman, 2002; Ramu et al., 2006; Ghosh et al., 2009a; Ogawa et al., 1990). Specialized devices for small animals have been improved over the years to generate excellent resolution images with high contrast between grey and white matter. A higher magnetic field strength than in the clinical setting allows a stronger signal and reduces voxel size (Bilgen, 2012), with field strengths up to 16.4T available (Brennan et al., 2013). Additionally, size-adjusted volume and surface coils achieve noise reduction and decrease the field of view for a higher signal to noise ratio (Bilgen, 2012). However, with varying field strength and for each imaging modality mentioned above the common acquisition parameters must be adjusted, which include but are not limited to repetition time, echo time, field of view and slice thickness (Bilgen, 2012).

4.1.3 Areas of application: MRI in SCI research is mostly used for the morphologic assessment of white matter pathology, including volumetric calculations of the lesion, and labeling of hyper- and hypointense areas as edema, hemorrhage or necrosis (Brennan et al., 2013; Sundberg et al., 2010; Song et al., 2018). The progression of the lesion volume over time can be assessed, displaying pathophysiological changes at both the epicenter and at areas rostral and caudal of the lesion, allowing for a prediction correlation to neurologic function (Wilkins et al., 2020). Following SCI, the integrity and regeneration of the Blood-Spinal-Cord-Barrier (BSCB) can also be assessed with MRI (Sundberg et al., 2011; Bilgen et al., 2001; Patel et al., 2009). Using Diffusion Tensor Imaging (DTI) technique, axonal integrity can be assessed (Tu et al., 2013). Another interesting area of application is the assessment of cortical plasticity following SCI using functional MRI (fMRI) (Ghosh et al., 2009a; Matsubayashi et al., 2018). This technique holds the ability to display the redistribution of somatosensory neurons in the cortex featuring the rewiring of hindlimb motoneurons (Ghosh et al., 2010). As a correlating technique Transcranial Magnetic Stimulation (TMS) has been shown to influence cortical plasticity, with both electromyography (EMG) and high-resolution fMRI detecting cortical responses to hindlimb stimulation in SCI animals, delivering promising results on enhancing neuronal plasticity and functional recovery (Krishnan et al., 2019). Additionally, MRI allows for the dynamic and non-invasive monitoring of stem cell migration after transplantation (Filippi et al., 2016; Gonzalez-Lara et al., 2011; Hu et al., 2012a; Shen et al., 2009). A selection of contrast agents to render stem cells MRI-detectable have been tested in rodent SCI models, most frequently superparamagnetic iron-oxide particles (SPIO) (Hu et al., 2012a; Shen et al., 2009; Gonzalez-Lara et al., 2009) and more recently Gadolinium-based (Gd) (Filippi et al., 2016; Yahyapour et al., 2018). While both show promising images of initial cell movements, signal loss is observed after about ten days with Gd agents, likely due to dilution from continuous cell division, as all contrast agents are administered *in vitro* (Filippi et al., 2016). SPIO signals were detectable up to three weeks post injection by Hu et al. (2012), but more susceptible to artifacts (Hu et al., 2012a). Guzman et al. (2007) have managed to trace SPIO-labeled stem cells for up to 18 weeks, however in the brain (Guzman et al., 2007).

4.1.4 Strengths and weaknesses: A good correlation of white matter integrity and regeneration with functional recovery could be demonstrated in studies using MRI, neurobehavioral analysis and histopathology (Wilkins et al., 2020). The rodent's physiological movements remain a problem, causing longer examination times as compared to humans (Schilling et al., 2019). Rodent studies therefore often use a small sample size, due to high cost and effort (Ramu et al., 2006; Filippi et al., 2016; Tu et al., 2010). To increase availability and reduce material costs, the use of clinical 1.5 –3 T MRI scanners in rodents has been investigated, most recently by Derksen et al. (2021) The authors performed fMRI on rats with a custom-designed coil in a clinical scanner. However, resulting voxel size and repetition time were inferior to specialized animal scanners (Derksen et al., 2021). Small animal scanners with a higher range of field strengths allow the imaging of spinal cord tissue in growing detail. Thus, contrast-labeled stem cells in the literature were traceable with 4.7 and 7 T scanners (Filippi et al., 2016; Gonzalez-Lara et al., 2011), whereas fMRI of neuronal pathways could be carried out at 9.4 T (Ghosh et al., 2010), and the exact location of responses to stimulation using targeted TMS therapy was evaluable by 11.1 T MRI (Krishnan et al., 2019). Clear differentiation of white and grey matter in the rodent spinal cord, including pathological changes, is indeed possible in clinical 2 T scanners - as was demonstrated as early as 1994 by Falconer et al. in the first longitudinal *in vivo* MRI study of murine SCI (Falconer et al., 1994). However, DTI allows quantitative assessment of white matter integrity, and Brennan et al. suggest that 16.4 T DTI detects changes in radial diffusivity better than a similar study carried out at 4.7 T, proposing a higher field strength beneficial (Brennan et al., 2013). MR images are stationary and cannot monitor dynamic changes in real-time, like in imaging methods discussed below (Brieu et al., 2010; Richards et al., 2017; Najafzadeh et al., 2020; Mallidi et al., 2011; Luke et al., 2012; Vawda et al., 2019; Badner et al., 2019). However, MRI still remains one of the most familiar and well-established imaging modality and is widely available (Farrar et al., 2012).

4.1.5 Outlook: Longitudinal *in vivo* rodent MRI provides the potential to explore microstructural damage and regeneration of the spinal cord following SCI (Duval et al., 2015). With DTI, axonal integrity and remyelination can potentially be assessed (Tu et al., 2013), while cortical plasticity following SCI can be examined using fMRI (Ghosh et al., 2009a; Matsubayashi et al., 2018) (Study overview: Table 1 (Patel et al., 2016; Brennan et al., 2013; Ghosh et al., 2010; Filippi et al., 2016; Endo et al., 2007; Ghosh et al., 2009b), Fig. 2: Examples of *in* and *ex vivo* MRI and volumetry in SCI.).

4.1.6 Potential for clinical translation: As clinical scanners predate specialized small animal scanners, availability does not pose an obstacle. Monitoring the development of the BSCB in patients may provide insight into an opportune moment for therapeutic intervention, while fMRI will help in understanding changes to ascending and descending pathways that can be targeted (Bakhsheshian et al., 2021).

4.2. Micro-Computed Tomography

4.2.1 History: In 1994, Micro-Computed Tomography (μCT) appeared in experimental use. Initially mostly used for high-resolution bone imaging *ex vivo*, the method found its application in experimental SCI rather recently (Xu et al., 2017; Hu et al., 2012b, 2015; Tschuchnig et al., 2021; Cao et al., 2017; Zambrano-Rodríguez et al., 2019). Although in SCI research μCT is mostly used *ex vivo* too (Xu et al., 2017; Hu et al., 2012b, 2015; Cao et al., 2017; Strotton et al., 2021), recent studies started with *in vivo* protocols to assess Spinal Subarachnoid Space (SSAS), or to monitor microangioarchitecture and posttraumatic tissue integrity, as well as stenosis of the spinal canal (Zambrano-Rodríguez et al., 2019, 2021a; Lee et al., 2012; Huang et al., 2020).

4.2.2 Technical: With μCT, a high-speed full-body scan can be performed in a small animal model with ultra-low X-ray radiation doses, with less than 2 mGy whole-body in a mouse. The technical background is the illumination of a sample with a micro-focus X-ray source. Through rotation and serial imaging acquiring 2D images, later 3D reconstruction and thus the complete imaging of a sample at high resolution can be achieved. This way in SCI, 3D-imaging of the micro-neurovascular anatomy or imaging of the SSAS can be achieved at a very high resolution, *in vivo* reported by Zambrano-Rodríguez et al. (2019) as 100 μm in rats (Hu et al., 2012b, 2015; Zambrano-Rodríguez et al., 2019, 2021a, 2021b; Cheng et al., 2015).

4.2.3 Areas of application: In SCI research, μCT is most frequently used *ex vivo* to 3D image explanted specimen (Hu et al., 2012b, 2015; Cao et al., 2017). One large field of use is the high-resolution imaging of bone quality in SCI induced sarcopenia (Otzel et al., 2019; Wu et al., 2021;

Table 1
Exemplary articles to the experimental usage of MRI and fMRI, Ultrasound, and *in vivo* Microscopy after Spinal Cord Injury.

MRI and fMRI					
Author (Date)	Animal	Injury model	Injury location	Imaging method	Primarily analyzed issue
Brennan et al. (2013)	C57BL/6 mice	Contusion	Thoracic, Th9	MRI, DTI	White matter pathology and regeneration
Endo et al. (2007)	Sprague-Dawley rats	Transection	Thoracic, Th9	BOLD fMRI	Cortical rewiring
Filippi et al. (2016)	Balb/c mice	Lateral hemisection	Lumbar, L2	MRI, DTI	Tracking of Gadoteridol-labeled Mesenchymal stem cells
Ghosh et al. (2009a, 2009b)	Lewis rats	Lateral hemisection	Cervical, C4	BOLD fMRI	Cortical rewiring
Ghosh et al. (2010)	Lewis rats	Transection	Thoracic, Th8	BOLD fMRI	Cortical rewiring
Patel et al. (2016)	Sprague-Dawley rats	Contusion	Thoracic, Th7	MRI	BSCB permeability
(Very High Resolution) Ultrasound					
Khaing et al., 2018	Sprague-Dawley rats	Compression	Thoracic, Th6-Th10	Ultrafast CEU	Hemodynamic changes
Soubeyrand et al. (2014a, 2014b)	Wistar rats	Clip Compression	Thoracic, Th10-Th12	VHRUS	Vascular injury and regeneration
Figley et al. (2013a, 2013b)	Athymic nude/C57BL/6 mice	Irradiation	Lumbar, L2-L3	VHRUS and PA	Vascular injury and regeneration
In vivo microscopy					
Kerschensteiner et al. (2005)	C57BL/6 mice	Transection	Cervical, C3–C6	WFFM	Axonal degeneration and regeneration
Farrar et al. (2012)	C57BL/6 mice (YFP-H)	Laser ablation	Thoracic, Th12	TPEF	Axonal degeneration and scar formation
Fenrich et al. (2013)	C57BL/6 mice	Unilateral Pinprick	Thoracic – Lumbar, Th12 – L2	TPEF	Infiltrating and resident myelomonocytic cells
Horiuchi et al. (2015)	B6.Cg-Tg (Thy1-YFP) H2Jrs/J mice	Contusion	Thoracic, Th11	TPEF	Axons of the dorsal funiculi
Chen et al. (2017a, 2017b)	Sprague Dawley rats	Contusion	Cervical, C7	TPEF	Vascular changes

Abbreviations: BOLD = Blood Oxygen Saturation Level, BSCB = Blood-Spinal-Cord-Barrier, C = Cervical vertebra, CEU = Contrast-Enhanced Ultrasound, DTI = Diffusion Tensor Imaging, fMRI = functional Magnetic Resonance Imaging, L = Lumbar vertebra, MRI = Magnetic Resonance Imaging, PA = Photoacoustic Imaging, Th = Thoracic vertebra, TPEF = Two Photon Excitation Fluorescence Microscopy, VHRUS = Very High Resolution Ultrasound, WFFM = Widefield Fluorescence Microscopy, YFP = Yellow Fluorescent Protein.

Yarrow et al., 2014; Debaud et al., 2017). *In vivo*, Zambrano-Rodríguez et al. were 2019 able to combine myelography with contrast-enhanced intravital μCT to image the SSAS in the rat and were later able to provide high-resolution *in vivo* images of changes in the SSAS following SCI (Zambrano-Rodríguez et al., 2019, 2021b). Moreover, μCT is used for the assessment of spinal canal width in a rodent model of spinal spondylotic myelopathy (Lee et al., 2012) and for the imaging of spinal cord integrity in therapy studies following SCI (Huang et al., 2020).

4.2.4 Strengths and weaknesses: In the *ex vivo* application, one strength of μCT is its non-destructiveness and therefore the preservation of samples for later destructive analyses like histology (Hu et al., 2012b, 2015; Cao et al., 2017). *In vivo*, the potential for high-resolution SSAS imaging has been shown. Also, tissue integrity following injury and the regeneration potential of SCI therapies was examined (Zambrano-Rodríguez et al., 2019, 2021b). In comparison to MRI, μCT image acquisition can be fast, but high-resolution 3D image reconstruction takes up to 5 h (Zambrano-Rodríguez et al., 2019, 2021a) and a complex IT infrastructure for image processing is necessary. Although μCT uses low radiation doses, repeated *in vivo* full body imaging of small animals can lead to relevant radiation exposure (Zambrano-Rodríguez et al., 2021b).

4.2.5 Outlook and potential for clinical translation: In addition to the beforementioned, interesting is the ability of modern μCT scanners to be combined with PET imaging and thus the multifold of possible experimental applications *in vivo*. In the clinic, μCT is reserved for high-resolution *ex vivo* sample analysis, for example in breast cancer and pulmonary diseases (Mai et al., 2017; Dicorpo, Tiwari, Tang, Griffin, Aftreth, Pinky BautistaHughes, Gershenfeld, Michaelson).

4.3. Laser Speckle Contrast Imaging

4.3.1 History: The fundamental principle of Laser Speckle Contrast Imaging (LSCI) evolved in the 1960s and 1970s (1976; Briers et al., 2013). Later on, it has been used for real-time imaging of blood flow mostly on the surface of the cortex in neuroscience and clinical research (Briers et al., 2013). Its usage for experimental application in SCI up to date is limited.

4.3.2 Technical: In LSCI, a laser light (coherent light, infrared or near infrared) throws light on an object with an irregular surface which is then reflected. This creates an interference pattern, called a speckle (Briers et al., 2013; Briers, 2001; Davis et al., 2014). The speckle approach was originally a single point measurement method; later scanning techniques were developed to provide a map of velocities (Briers et al., 2013; Briers, 2001). The theory of laser speckle contrast analysis is based on the principle that motion causes alterations in the speckle pattern, as for the movement of blood cells. Fast flow leads to a more indistinct pattern while the contrast is diminished whereas a decrease in flow is associated with higher contrast (Briers, 2001; Hecht et al., 2009; Lesage et al., 2009). Cameras detect the speckle pattern, and contrast can be calculated. Based on that, contrast calculating software is able to create a color-coded map for example of blood flow velocities (Hecht et al., 2009; Senarathna et al., 2013). However, imaging depth remains low, creating a momentary map of surface vascular anatomy (Senarathna et al., 2013; Gallagher et al., 2019). Depending on the wavelength the tissue can be penetrated by less than 1 mm and a spatial resolution of about 10 μm can be achieved (Senarathna et al., 2013).

4.3.3 Areas of Application: LSCI is mostly used to map superficial vessels in the cortex and less to image deep vessels in the spinal cord (Senarathna et al., 2013). Thus, LSCI is rarely used in experimental spinal cord imaging compared to its wide usage in measuring the blood flow of the cortex (Lesage et al., 2009; Dunn et al., 2005; Luo et al., 2007; Woitzik et al., 2013). Reason for this is mostly the limited depth of this technique and the challenge of respiration artifacts (Lesage et al., 2009). However, some SCI researchers used this tool to measure the restoration of spinal cord blood flow following electrical stimulation, or for imaging the superficial vascular reaction to neuronal stimulation in injured and non-injured rodents (Lesage et al., 2009; Beaumont et al., 2014; Brieu et al., 2010).

4.3.4 Strengths and Weaknesses: LSCI is a non-invasive, real-time technique which enables full-field imaging in 2-dimension. The equipment is well accessible (common laser, optics, and camera) at relatively low cost. An additional contrast agent is not required (Briers, 2001; Richards et al., 2017; Murari et al., 2007). Although the spatial and temporal resolution of this imaging technique is high, imaging depth remains low, making the technique not suitable for imaging deeper

vascular networks in the spinal cord (Lesage et al., 2009; Senarathna et al., 2013).

4.3.5 Outlook and potential for clinical translation: Although widely used in the clinic and in the laboratory for cortical surface blood flow analysis, the use of LSCI for clinical and experimental application in SCI remains limited.

4.4. Very high resolution ultrasound and Photoacoustic Imaging

4.4.1 History: The use of Very High Resolution Ultrasound (VHRUS) as an *in vivo* imaging tool in SCI has emerged over the last decade. With a trend towards the use of higher frequency ultrasound, a higher spatial resolution can be achieved. Moreover, a combination with other techniques like contrast-enhanced Ultra-sonography and Photoacoustic Imaging (PA) is available (Xu and Wang, 2006). This makes VHRUS an inexpensive and user-friendly tool for *in vivo* imaging of the whole spinal cord following SCI (Soubeyrand et al., 2012, 2014b; Figley et al., 2013a).

4.4.2 Technical: VHRUS is possible with specialized ultrasound machines (Soubeyrand et al., 2014a, 2014b). Using a high frequency (40–50 MHz), high resolution with 20–30 microns per pixel can be achieved (Soubeyrand et al., 2012; Finn-Bodner et al., 1995; Huang et al., 2013; Jones et al., 2012; Dubory et al., 2015). Contrast-enhanced ultrasonography is possible via the intravenous administration of microbubbles serving as a contrast-agent (Soubeyrand et al., 2012; Dubory et al., 2015). Compared to other functional vessel imaging like MR-angiography or CT-angiography, emerging ultrasound techniques allow for a higher resolution and co-registering with Photoacoustic Imaging (PA) is possible (Khaing et al., 2018). PA is based on the physical principle of the photoacoustic effect, initially reported in 1880. With this technique, non-invasive image-based oxygen saturation measuring in spinal cord vessels and spinal cord tissue is possible to assess hypoxia and ischemia (Xu and Wang, 2006; Figley et al., 2013b; Bell, 1880). In PA, absorption by the target molecule leads to a local temperature rise and therefore to thermal expansion of the tissue producing acoustic waves recognized by an ultrasound transducer (Najafzadeh et al., 2020; Mallidi et al., 2011). Distinct absorption properties apply to various optical chromophores (i.e. oxygenated or deoxygenated hemoglobin, melanin, water, and lipid) (Jeon et al., 2016). An additional combination with contrast agents like contrast dyes or nanoparticles is possible to increase the photoacoustic signal (Xu and Wang, 2006; Luke et al., 2012). With appropriate contrast agents, imaging on the cellular and even molecular level is realizable (Najafzadeh et al., 2020; Mallidi et al., 2011; Jeon et al., 2016). Also, the technique allows for 3D tissue imaging (Soubeyrand et al., 2014a; Moonen et al., 2016; Vawda et al., 2019).

4.4.3 Areas of Application: In experimental SCI, VHRUS can be used to longitudinally quantify the posttraumatic morphological alterations as well as changes in hemodynamics in the spinal cord (Moonen et al., 2016; Badner et al., 2019). Parameters thus assessable include lesion volume, cavity volume, parenchymal hemorrhage and alterations in spinal cord blood flow (Soubeyrand et al., 2014b; Dubory et al., 2015; Khaing et al., 2018). Additionally, the migration of infused mesenchymal stem cells can be examined (Vawda et al., 2019; Soubeyrand et al., 2014c). In combination with PA, oxygen saturation of the spinal cord tissue and vasculature can be non-invasively assessed (Figley et al., 2013b; Soubeyrand et al., 2014c). Thus, using VHRUS the effects of potential neuroprotective and regenerative treatments such as norepinephrine and mesenchymal stomal cells could previously be assessed (Vawda et al., 2019; Soubeyrand et al., 2014c) and the role of IL-10 in the vascular pathology of SCI could be examined (Badner et al., 2019).

4.4.4 Strengths and Weaknesses: VHRUS allows for low-invasive, real-time longitudinal *in vivo* 3D-imaging of the whole spinal cord with high resolution and high depth (Vawda et al., 2019; Soubeyrand et al., 2014c). Some investigators perform repetitive surgery for VHRUS application on top of the dura. However, more modern technique allows the non-invasive application of VHRUS through the skin. Using ultrasound, tissue morphology is preserved and unaltered post mortem tissue processing remains possible (Soubeyrand et al., 2014b; Moonen et al., 2016). Apart from the VHRUS machine, the technique is inexpensive, with manageable recourses necessary. Image acquisition is fast and can easily be adjusted (Soubeyrand et al., 2014b; Dubory et al., 2015). PA and contrast-enhanced imaging can be combined, allowing for accurate and rapid monitoring of effects of prospective treatments targeting spinal cord regeneration (Soubeyrand et al., 2014a, 2014c; Dubory et al., 2015; Vawda et al., 2019).

4.4.5 Experimental outlook: VHRUS is a fast and easily adjustable technique for longitudinal 3D *in vivo* imaging of the whole spinal cord (Soubeyrand et al., 2014a). The combination with contrast-enhanced ultrasonography allows for the tracking of blood flow and for cell tracking, whereas the combination with PA allows for non-invasive oxygen saturation measurement in the spinal cord and spinal cord vasculature (Soubeyrand et al., 2014a; Figley et al., 2013b). The trend with ultrasound techniques goes towards higher frequencies leading to even higher resolution (Dubory et al., 2015) (Study overview: Table 2 (Soubeyrand et al., 2014b; Khaing et al., 2018; Figley et al., 2013b), Schematic setup of VHRUS and exemplary images in B-Mode and Power Doppler Mode: Fig. 3.).

4.4.6 Potential for clinical translation: To monitor spinal cord blood flow following injury in humans with minimally-invasive ultrasound techniques is of interest (Chen et al., 2017a; Khaing et al., 2020), as the hemodynamic stability and an intact perfusion of the spinal cord is associated with an improved outcome regarding functionality (Werndle et al., 2014; Tator, 1991). Another potential translational approach to integrate ultrasound in combination with specific contrast agents could allow molecular imaging in clinical SCI (Khaing et al., 2020). In a preclinical model targeted contrast-enhanced ultrasound (TCEUS) was already described as a promising tool for the future (Volz et al., 2016, 2017).

4.5. Spinal cord microscopy

4.5.1 History: The first experimental tool used for *in vivo* microscopy was wide field fluorescence microscopy (WFFM), also called *in vivo* Epifluorescence Videomicroscopy (IVM), a basic microscope technique to image fluorescence (Kerschensteiner et al., 2005; Misgeld et al., 2007; Vajkoczy et al., 2001). However, due to limited penetration depth and limited axial resolution, the technique developed further. Two-photon excitation fluorescence microscopy (TPEF) was established in 1990, and first used in animal experiments to image glial cells in the brain (Helmchen and Denk, 2005; Denk et al., 1990). Later, TPEF was used for the tracking of immune cells in various organs. After many *ex vivo* studies it was first used *in vivo* 2003 for the imaging of lymphocytes (Cahalan et al., 2003). Originally only used for imaging cell movement, TPEF was later on also used with fluorescent proteins to image cell functions *in vivo* (Kawakami, 2018). Up to date, TPEF has become one of the superior tools for *in vivo* imaging.

4.5.2 Technical: *In vivo* imaging of the spinal cord is possible following surgical removal of the laminae (laminectomy), and for longitudinal *in vivo* imaging can be combined with the implantation of a spinal window chamber (Farrar et al., 2012; Figley et al., 2013b; Fenrich et al., 2012). In Epifluorescence Videomicroscopy (IVM), the specimen is exposed to light while illumination and detection of light cover the whole visual field simultaneously. The light source can be an LED, Mercury or Xenon arc-lamp, combined with an optical filter to choose wavelength. The image is captured by camera. Out of focus light and diffraction-limited optics result in comparably low contrast. Therefore, layers of single cells or organelles are best suited for this imaging modality (Sanderson et al., 2014). Two-photon excitation fluorescence microscopy (TPEF) is a non-linear optical method, based on photon excitation. Two photons of the same wavelength excite a fluorophore simultaneously. Together, they create enough energy for the emission of a single fluorescence photon with a higher level of energy and with shorter wavelength. This represents one pixel in the image. A

femtosecond pulsated laser as light source with an optimum range at 800 nm (650–1000 nm) generates ultrashort impulses (<100 fsec) at 100 MHz and is pumped with another laser (around 500 nm). This way, a tissue penetration depth of around 600 nm is created (Helmchen and Denk, 2005; Johannssen and Helmchen, 2013). With even higher impulse energy systems, up to 1000 μm depth was previously achieved in the murine cortex (Theer et al., 2003).

4.5.3 Areas of application: Transgenic mice have been frequently used with IVM, for example YFP-labeled (yellow-fluorescent protein, H-line of thy1-YFP) (Misgeld et al., 2007; Skuba et al., 2011). As blood vessels originally appear dark, fluorescent dyes like rhodamine or FITC were also frequently administered intravenously (Dray et al., 2009; Chen et al., 2017b). This makes the tool relevant for the examination of structures rarely covered with tissue, like dorsal root ganglia (DRG) after laminectomy, the imaging of vessels and the continual tracing of axons and their de- and regeneration (Kerschensteiner et al., 2005). TPEF is increasingly used for spinal cord imaging in recent years. Mostly the dorsal funiculi and DRG have been imaged, with a penetration depth of 150–300 μm (Laskowski and Bradke, 2013). So far, imaging studies using TPEF in the spinal cord have examined cellular migration with microglia and macrophages (Evans et al., 2014) or bone-marrow derived stromal cells (Cord et al., 2005), dynamic vascular changes (Dray et al., 2009; Chen et al., 2017b; Davalos and Akassoglou, 2012; Tang et al., 2015), vascular damage (Zhang et al., 2014; Yang et al., 2017a) and neuronal and axonal degeneration and regeneration (Dray et al., 2009; Horiuchi et al., 2015; Zhang et al., 2015). Different fluorescent dyes and fluorescent transgenic mouse lines can be combined with this imaging method. The use of fluorescent dyes coupled to molecules of different sizes (e.g. dextran) further allows for the assessment of extravasation kinetics and a detailed analysis of BSCB (blood-spinal-cord-barrier) function and integrity. Frequently used transgenic mouse lines possess promotors coupled to fluorescent proteins YFP to image motor and sensory neurons and/or GFP (green fluorescent protein) to image mononuclear cells (Horiuchi et al., 2015). Moreover, SCa1-I_{REF} can be used for imaging Ca^{2+}-dynamics in live neurons, while Adeno-Associated Virus (AAV) expressing a fluorophore (e.g. GFP) can function as a tracer for axon-regeneration (Liao et al., 2017; Uckermann et al., 2015; Galli et al., 2018).

To assess axonal degeneration and regeneration following SCI, *in vivo* imaging of YFP-labeled axons allows for the visualization and quantification of acute axonal degeneration and Wallerian degeneration. The combination of TPEF microscopy with Third Harmonic Generation microscopy reveals the spatially and temporally overlapped degeneration of axons and myelin after SCI (Farrar et al., 2011a). Recently, the formation and dynamic change of spheroids has been examined, thereby further characterizing the acute axonal degeneration post injury (Orem et al., 2020a, 2020b). To further understand the pathophysiological processes underlying axonal degeneration, intracellular Ca2+ levels were quantified using mice containing the GFP-positive calcium indicator GCaMP6f in axons (Orem et al., 2020b; Tang, Zhang, Chen, Xinran, Ju, Liu, Gan, He, Zhang, Li, Zhang, Kirby). Some of the parameters mentioned above were also used to show the therapeutic effects of e.g. Methylprednisolone and Progesterone on axonal survival *in vivo* (Zhang et al., 2015; Orem et al., 2020a; Tang, Zhang, Chen, Xinran, Ju, Liu, Gan, He, Zhang, Li, Zhang, Kirby; Yang et al., 2017b). To examine vascular changes post SCI, most studies imaging vasculature via TPEF microscopy *in vivo* use the visualization of vessels as orientation and show the interaction with extraluminal cells like microglia or axons (Davalos and Akassoglou, 2012; Oshima et al., 2014; Fenrich et al., 2013). Also, *in vivo* imaging of cell migration is possible with labeled macrophages (Farrar et al., 2012; Evans et al., 2014; Fenrich et al., 2013; Davalos, Lee, Smith, Brinkman, Ellisman, Zheng, Akassoglou).

4.5.4 Strengths and Weaknesses: Although IVM is limited in penetration depth, its easy technique allows for fast noninvasive *in vivo* imaging of the Spinal Cord (Shi et al., 2019). SCI as in lesion models (transection, crush, or compression contusion injury) can be thus directly confirmed. Fast camera speed and recording is possible almost without respiratory interruptions and with low phototoxicity (Misgeld et al., 2007). Due to the limited penetration depth of this technique, imaging of the spinal cord vasculature and spinal cord neurons is possible in superficial areas of the dorsal spinal cord. *In vivo* microscopy enables longitudinal imaging over longer time periods. In combination with the sophisticated implantation of a spinal window chamber, repetitive surgery to expose the spinal cord has become obsolete (Farrar et al., 2012; Figley et al., 2013b; Fenrich et al., 2012). In TPEF, enhanced imaging depth is enabled by longer wavelength, which results in less scattering artifacts and less absorption within the tissue, compared to other *in vivo* microscopy techniques. The technique also further reduces the probability of phototoxicity, with no out-of-focus tissue bleaching. It allows for the differentiation between spared axons and regenerated sprouts as well as between spared and regenerated vessels and enables a direct evaluation of therapeutic effects. Alterations however are caused by breathing and pulse, though many attempts exist to deal with these artifacts (Davalos and Akassoglou, 2012).

4.5.5 Experimental outlook: TPEF has become one of the superior tools for experimental *in vivo* imaging, thanks to its high resolution and the possibility for longitudinal imaging without repetitive surgery with the usage of sophisticated spinal window chambers. A magnitude of different fluorescent dyes and transgenic mouse lines enables real-time *in vivo* imaging of complex pathophysiological processes like axonal de- and regeneration, neuronal Ca^{2+}-signaling, and vessel restoration and function and much more following SCI. TPEF can be integrated with further nonlinear contrast imaging modalities for more specific purposes like Second Harmonic generation microscopy (SHG), used for the imaging of neuronal repair and fibrotic scar formation (Horiuchi et al., 2015; Liao et al., 2017). Third harmonic generation microscopy (THG) and Coherent Anti stokes Raman Scattering (CARS) have been used to image lipids and myelin structures to examine de- and remyelination (Farrar et al., 2011b; Hu et al., 2014; Galli et al., 2012) (Study overview: Table 3 (Farrar et al., 2012; Kerschensteiner et al., 2005; Horiuchi et al., 2015; Fenrich et al., 2013; Wang et al., 2017), Fig. 4: *In vivo* IVM via implanted spinal window chamber and schematic setup of TPEF).

4.5.6 Potential for clinical translation: Even if TPEF microscopy is most often used in an experimental setting, it already contributes to clinical diagnostics. In the clinical setting it can be used to image human tissue *ex vivo* for example in the field of oncology (Li et al., 2018). The clinical intravital use of TPEF microscopy is only well established in dermatology. Here it is a useful tool to image skin disease like melanoma (Dimitrow et al., 2009). Intravital TPEF microscopy has also been used in single cases in other surgical fields like in brain tumor surgery (Kantelhardt et al., 2016). Wide-field fluorescence microscopy is not fully translated to the clinic but is tested as a diagnostic tool in the point of care of e.g. Barret's neoplasia (Joshi et al., 2016) or colon cancer (Sensarn et al., 2016). For this application classical point of care white light endoscopes are modified to detect the specific fluorescence signals.

5. Discussion and limitations

Knowing about the different *in vivo* imaging methods available in an experimental setting today to monitor spinal cord injury and spinal cord regeneration helps with an overview about the potentials these methods hold to improve pathophysiological knowledge and thus to enhance regenerative therapies. However, for detailed experimental planning it is important to look at this multifold of imaging methods and techniques available regarding the intended study goal to monitor specific pathophysiological changes and regeneration. Thus, not all the mentioned methods hold the same potentials and limitations, as mentioned in the sections above. Moreover, between different techniques of the same imaging method, e.g. different MRI scanners or different MRI sequences, or different VHRUS machines of different generations there exist relevant differences. In the planning of an experiment, these details need to be assessed and dealt with. The goal of this review is to give an overview

about the multiple options available, but one possible limitation is that a more detailed review of the different subsets of every discussed imaging technique is not achieved.

Moreover, there exist multiple established experimental models for experimental SCI induction in rodents, and even between rats and mice, there exist relevant differences in SCI pathophysiology. The reviewed studies include different animal models, like weight drop injury, impactor model, clip compression contusion injury, forceps injury, hemisection, or irradiation, in mice and rats. The one specific imaging method for the one injury model or animal model is not existent and methodological heterogeneity in the analyzed studies is high. In Table 1, exemplary studies included in the data synthesis are displayed, with the information which specimen and which SCI model was used. In experimental planning, the planned use of specimen, SCI model and combined imaging method is important regarding the intended study goal. The lack of differentiation thus is another potential limitation of this review.

6. Conclusions

Experimental studies using longitudinal *in vivo* imaging play a significant role in the characterization of potential targets for advancing spinal cord regeneration. Techniques at hand for *in vivo* imaging in SCI have dynamically evolved over the past decades. With the use of advanced imaging techniques like high-resolution MRI and fMRI combined with TMS, μCT, Very High Resolution Ultrasound combined with Contrast-Enhanced or Photoacoustic Imaging, and Two-Photon Excitation Fluorescence Microscopy in combination with various fluorescent dyes and transgenic mouse lines, longitudinal real-time *in vivo* imaging of neuronal, vascular and cellular regeneration of the spinal cord is possible non-invasively. With this study we comprehensively review experimental setups using *in vivo* imaging of different kind in SCI, to give an up-to-date overview to experimental researchers thriving to advance the knowledge on spinal cord regeneration and repair following SCI. A thorough knowledge of the strengths and limitations of these techniques will help to optimally exploit our current experimental armamentarium in the field.

Author's disclosure statement

No conflicts of interest exist in the submission of the manuscript and the manuscript is approved by all authors for publication.

Funding

No special funding was received for this study. VH was supported by the 2019 Integra EANS research fund and is currently funded by the BIH Charité Clinician Scientist program.

Declaration of competing interest

The authors declare that they have no known competing financial interests or personal relationships that could have appeared to influence the work reported in this paper.

Acknowledgements

PV and VH designed the study concept. VH, LM, LR and LW performed the systematic literature review and data analysis, participated in data acquisition, and wrote the manuscript. MN helped with the acquisition of the *in vivo* images. PV and MGF evaluated the data and revised the manuscript.

Abbreviations

μCT	Micro-Computed Tomography
3D	3 Dimensional
AAV	Adeno-Associated Virus
BOLD	Blood Oxygen Level Dependent
BSCB	blood-spinal cord barrier
CARS	Coherent Anti stokes Raman Scattering
CEU	Contrast-Enhanced Ultrasonography
CT	Computed Tomography
CNS	Central Nervous System
DRG	Dorsal root ganglia
DTI	Diffusion Tensor Imaging
EMG	electromyography
FITC	Fluorescent isothiocyanate
fMRI	functional Magnetic resonance imaging
GFP	Green-fluorescent protein
^{1}H-MRS	proton magnetic resonance spectroscopy
LED	Light Emitting Diode
LSCI	Laser Speckle Contrast Imaging
MRI	Magnetic resonance imaging
MSCs	mesenchymal stem cells
PA	Photoacoustic Imaging
PRISMA	Preferred Reporting Items for Systematic Reviews and Meta-Analyses
RARE	Rapid Acquisition with Relaxation Enhancement
RSE	Rapid Spin Echo
SCBF	Spinal Cord Blood Flow
SCI	Spinal Cord Injury
SHG	Second Harmonic generation microscopy
SNR	Signal-to-noise-ratio
SSAS	Spinal Subarachnoid Space
T	Tesla
THG	Third harmonic generation microscopy
TMS	transcortical magnetic stimulation
TPEF	two-photon excitation microscopy
VHRUS	Very High Resolution Ultrasound
YFP	Yellow-fluorescent protein

References

Badhiwala, J.H., Wilson, J.R., Fehlings, M.G., 2018. Global burden of traumatic brain and spinal cord injury. Lancet Neurol. 18, 24–25.

Badner, A., Vawda, R., Laliberte, A., Hong, J., Mikhail, M., Jose, A., Dragas, R., Fehlings, M., 2016. Fetal and neonatal stem cells early intravenous delivery of human brain stromal cells modulates systemic inflammation and leads to vasoprotection in traumatic spinal cord injury. Stem Cells Transl. Med. 5, 991–1003.

Badner, A., Vidal, P.M., Hong, J., Hacker, J., Fehlings, M.G., 2019. Endogenous interleukin-10 deficiency exacerbates vascular pathology in traumatic cervical spinal cord injury. J. Neurotrauma 36, 2298–2307.

Bakhsheshian, J., Strickland, B.A., Mack, W.J., Zlokovic, B.V., 2021. Investigating the blood–spinal cord barrier in preclinical models: a systematic review of in vivo imaging techniques. Spinal Cord 59, 596–612.

Basser, P.J., Mattiello, J., LeBihan, D., 1994. MR diffusion tensor spectroscopy and imaging. Biophys. J. 66, 259–267.

Beaumont, E., Guevara, E., Dubeau, S., Lesage, F., Nagai, M., Popovic, M., 2014. Functional electrical stimulation post-spinal cord injury improves locomotion and increases afferent input into the central nervous system in rats. J. Spinal Cord Med. 37, 93–100.

Bell, A.G., 1880. On the production and reproduction of sound by light. Am. J. Sci. 20, 305–324.

Bilgen, M., 2012. Neuroimaging assessment of spinal cord injury in rodents. In: Animal Models of Acite Neurological Injuries II. Springer Protocols Handbooks, pp. 679–698.

Bilgen, M., Abbe, R., Narayana, P.A., 2001. Dynamic contrast-enhanced MRI of experimental spinal cord injury: in vivo serial studies. Magn. Reson. Med. 45, 614–622.

Brennan, F.H., Cowin, G.J., Kurniawan, N.D., Ruitenberg, M.J., 2013. Longitudinal assessment of white matter pathology in the injured mouse spinal cord through ultra-high field (16.4T) in vivo diffusion tensor imaging. Neuroimage 82, 574–585.

Briers, J.D., 2001. Laser Doppler, speckle and related techniques for blood perfusion mapping and imaging. Physiol. Meas. 22.

Briers, D., Duncan, D.D., Hirst, E., Kirkpatrick, S.J., Larsson, M., Steenbergen, W., Stromberg, T., Thompson, O.B., 2013. Laser speckle contrast imaging: theoretical and practical limitations. J. Biomed. Opt. 18, 066018.

Brieu, N., Beaumont, E., Dubeau, S., Cohen-Adad, J., Lesage, F., 2010. Characterization of the hemodynamic response in the rat lumbar spinal cord using intrinsic optical imaging and laser speckle. J. Neurosci. Methods 191, 151–157.

Cahalan, M., Parker, I., Wei, S., Miller, M., 2003. Real-time imaging of lymphocytes in vivo Michael. Curr. Opin. Immunol. 15, 372–377.

Cao, Y., Wu, T., ding, Wu, H., Lang, Y., Li, D. zhe, Ni, S. fei, Lu, H. Bin, Hu, J.Z., 2017. Synchrotron radiation micro-CT as a novel tool to evaluate the effect of agomir-210 in a rat spinal cord injury model. Brain Res. 1655, 55–65.

Chen, S., Smielewski, P., Czosnyka, M., Papadopoulos, M.C., Saadoun, S., 2017a. Continuous monitoring and visualization of optimum spinal cord perfusion pressure in patients with acute cord injury. J. Neurotrauma 34.

Chen, C., Zhang, Y.P., Sun, Y., Xiong, W., Shields, L.B., Shields, C.B., Jin, X., Xu, X.M., 2017b. An in vivo duo-color method for imaging vascular dynamics following contusive spinal cord injury. J. Vis. Exp., 56565

Cheng, X., Long, H.Q., Chen, W.L., Xu, J.H., Huang, Y.L., Li, F.B., 2015. Three-dimensional alteration of cervical anterior spinal artery and anterior radicular artery in rat model of chronic spinal cord compression by micro-CT. Neurosci. Lett. 606, 106–112.

Cohen, D.M., Patel, C.B., Ahobila-Vajjula, P., Sundberg, L.M., Chacko, T., Liu, S.-J., Narayana, P.A., 2009. Blood-spinal cord barrier permeability in experimental spinal cord injury: dynamic contrast-enhanced magnetic resonance imaging. NMR Biomed. 22, 332–341.

Cord, R.S., Yano, S., Kuroda, S., Lee, J., Shichinohe, H., Seki, T., Ikeda, J.U.N., Nishimura, G., Hida, K., 2005. In Vivo Fluorescence Tracking of Bone Marrow Stromal, vol. 22, pp. 907–918.

Cripps, R., Lee, B., Wing, P., Weerts, E., Mackay, J., Brown, D., 2010. A global map for traumatic spinal cord injury epidemiology: towards a living data repository for injury prevention. Spinal Cord 49, 493–501.

Davalos, D., Akassoglou, K., 2012. In vivo imaging of the mouse spinal cord using two-photon microscopy. JoVE 59.

Davalos, D., Lee, J.K., Smith, B., Brinkman, B., Ellisman, M.H., Zheng, B., and Akassoglou, K. ([date unknown]). Stable in Vivo Imaging of Densely Populated Glia, Axons and Blood Vessels in the Mouse Spinal Cord Using Two-Photon Microscopy.

Davis, M.A., Kazmi, S.M.S., Dunn, A.K., 2014. Imaging depth and multiple scattering in laser speckle contrast imaging. J. Biomed. Opt. 19, 086001.

Debaud, C., Salga, M., Begot, L., Holy, X., Chedik, M., De L'Escalopier, N., Torossian, F., Levesque, J.P., Lataillade, J.J., Le Bousse-Kerdilès, M.C., Genêt, F., 2017. Peripheral denervation participates in heterotopic ossification in a spinal cord injury model. PLoS One 12.

Denk, W., Strickler, J., Webb, W., 1990. Two-photon laser scanning fluorescence microscopy. Science 80 (248), 73–76.

Derksen, M., Rhemrev, V., van der Veer, M., Jolink, L., Zuidinga, B., Mulder, T., Reneman, L., Nederveen, A., Feenstra, M., Willuhn, I., Denys, D., 2021. Animal studies in clinical MRI scanners: a custom setup for combined fMRI and deep-brain stimulation in awake rats. J. Neurosci. Methods 360, 109240.

Dicorpo, D., Tiwari, Ankur, Tang, R., Griffin, M., Aftreth, O., Pinky Bautista, Hughes, K., Gershenfeld, · Neil, and Michaelson, James ([date unknown]). The Role of Micro-CT in Imaging Breast Cancer Specimens.vol. 1, 3.

Dimitrow, E., Ziemer, M., Koehler, M.J., Norgauer, J., König, K., Elsner, P., Kaatz, M., 2009. Sensitivity and specificity of multiphoton laser tomography for in Vivo and ex vivo diagnosis of malignant melanoma. J. Invest. Dermatol. 129, 1752–1758.

Dray, C., Rougon, G., Debarbieux, F., 2009. Quantitative analysis by in vivo imaging of the dynamics of vascular and axonal networks in injured mouse spinal cord. Proc. Natl. Acad. Sci. U.S.A. 106, 9459–9464.

Dubory, A., Laemmel, E., Badner, A., Duranteau, J., Vicaut, E., Court, C., Soubeyrand, M., 2015. Contrast enhanced ultrasound imaging for assessment of spinal cord blood flow in experimental spinal cord injury. J. Vis. Exp., 52536

Dunn, A.K., Devor, A., Dale, A.M., Boas, D.A., 2005. Spatial extent of oxygen metabolism and hemodynamic changes during functional activation of the rat somatosensory cortex. Neuroimage 27, 279–290.

Duval, T., McNab, J., Setsompop, K., Witzel, T., Schneider, T., Huang, S., Keil, B., Klawiter, E., Wald, L., Cohen-Adad, J., 2015. In Vivo Mapping of Human Spinal Cord Microstructure at 300 mT/m, pp. 494–507.

Endo, T., Spenger, C., Tominaga, T., Brené, S., Olson, L., 2007. Cortical sensory map rearrangement after spinal cord injury: fMRI responses linked to Nogo signalling. Brain 130, 2951–2961.

Evans, T.A., Barkauskas, D.S., Myers, J., Hare, E.G., You, J., Ransohoff, R.M., Huang, A.Y., Silver, J., Huang, A., 2014. High-resolution intravital imaging reveals that blood derived macrophages but not resident microglia facilitate secondary axonal dieback in traumatic spinal cord injury. Exp. Neurol. 254, 109–120.

Falconer, J.C., Narayana, P.A., Bhattacharjee, M.B., Liu, S.-J., 1994. Quantitative MRI of spinal cord injury in a rat model. Magn. Reson. Med. 32, 484–491.

Farrar, M.J., Wise, F.W., Fetcho, J.R., Schaffer, C.B., 2011b. In vivo imaging of myelin in the vertebrate central nervous system using third harmonic generation microscopy. Biophys. J. 100, 1362–1371.

Farrar, M.J., Wise, F.W., Fetcho, J.R., Schaffer, C.B., 2011b. In vivo imaging of myelin in the vertebrate central nervous system using third harmonic generation microscopy. Biophys. J. 100, 1362–1371.

Farrar, M.J., Bernstein, I.M., Schlafer, D.H., Cleland, T.A., Fetcho, J.R., Schaffer, C.B., 2012. Chronic in vivo imaging in the mouse spinal cord using an implanted chamber. Nat. Methods 9, 297–302.

Fenrich, K.K., Weber, P., Hocine, M., Zalc, M., Rougon, G., Debarbieux, F., 2012. Long-term in vivo imaging of normal and pathological mouse spinal cord with subcellular resolution using implanted glass windows. J. Physiol. 590, 3665–3675.

Fenrich, K.K., Weber, P., Rougon, G., Debarbieux, F., 2013. Long- and short-term intravital imaging reveals differential spatiotemporal recruitment and function of myelomonocytic cells after spinal cord injury. J. Physiol. 591, 4895–4902.

Figley, S.A., Chen, Y., Maeda, A., Conroy, L., Mcmullen, J.D., Silver, J.I., Stapleton, S., Vitkin, A., Lindsay, P., Burrell, K., Zadeh, G., Fehlings, M.G., Dacosta, R.S., 2013a. A spinal cord window chamber model for in vivo longitudinal multimodal optical and acoustic imaging in a murine model. PLoS One 8, 1–14.

Figley, S.A., Chen, Y., Maeda, A., Conroy, L., McMullen, J.D., Silver, J.I., Stapleton, S., Vitkin, A., Lindsay, P., Burrell, K., Zadeh, G., Fehlings, M.G., DaCosta, R.S., 2013b. A spinal cord window chamber model for in vivo longitudinal multimodal optical and acoustic imaging in a murine model. PLoS One 8.

Figley, S.A., Liu, Y., Karadimas, S.K., Satkunendrarajah, K., Fettes, P., Spratt, S.K., Lee, G., Ando, D., Surosky, R., Giedlin, M., Fehlings, M.G., 2014. Delayed administration of a bio-engineered zinc-finger VEGF-A gene therapy is neuroprotective and attenuates allodynia following traumatic spinal cord injury. PLoS One 9.

Filippi, M., Boido, M., Pasquino, C., Garello, F., Boffa, C., Terreno, E., 2016. Successful in vivo MRI tracking of MSCs labeled with Gadoteridol in a Spinal Cord Injury experimental model. Exp. Neurol. 282, 66–77.

Finn-Bodner, S.T., Hudson, J.A., Coates, J.R., Sorjonen, D.C., Simpson, S.T., Cox, N.R., Wright, J.C., Garrett, P.D., Steiss, J.E., Vaughn, D.M., Miller, S.C., Brown, S.A., 1995. Ultrasonographic anatomy of the normal canine spinal cord and correlation with histopathology after induced spinal cord trauma. Vet. Radiol. Ultrasound 36, 39–48.

Ford, J.C., Hackney, D.B., Joseph, P.M., Phelan, M., Alsop, D.C., Tabor, S.L., Hand, C.M., Markowitz, R.S., Black, P., 1994. A method for in vivo high resolution MRI of rat spinal cord injury. MRM 31, 218–223.

Forgione, N., Chamankhah, M., Fehlings, M.G., 2017. A mouse model of bilateral cervical contusion-compression spinal cord injury. J. Neurotrauma 34, 1227–1239.

Gallagher, M.J., Hogg, F.R.A., Zoumprouli, A., Papadopoulos, M.C., Saadoun, S., 2019. Spinal cord blood flow in patients with acute spinal cord injuries. J. Neurotrauma 36, 919–929.

Galli, R., Uckermann, O., Winterhalder, M.J., Sitoci-Ficici, K.H., Geiger, K.D., Koch, E., Schackert, G., Zumbusch, A., Steiner, G., Kirsch, M., 2012. Vibrational spectroscopic imaging and multiphoton microscopy of spinal cord injury. Anal. Chem. 84, 8707–8714.

Galli, R., Sitoci-Ficici, K.H., Uckermann, O., Later, R., Marečková, M., Koch, M., Leipnitz, E., Schackert, G., Koch, E., Gelinsky, M., Steiner, G., Kirsch, M., 2018. Label-free multiphoton microscopy reveals relevant tissue changes induced by alginate hydrogel implantation in rat spinal cord injury. Sci. Rep. 8, 1–13.

Ghosh, A., Sydekum, E., Haiss, F., Peduzzi, S., Zörner, B., Schneider, R., Baltes, C., Rudin, M., Weber, B., Schwab, M.E., 2009a. Functional and anatomical reorganization of the sensory-motor cortex after incomplete spinal cord injury in adult rats. J. Neurosci. 29, 12210–12219.

Ghosh, A., Sydekhum, E., Haiss, F., Peduzzi, S., Zörner, B., Schneider, R., Baltes, C., Rudin, M., Weber, B., Schwab, M., 2009b. Functional and anatomical reorganization of the sensory-motor cortex after incomplete spinal cord injury in adult rats. J. Neurosci. 29, 12210–12219.

Ghosh, A., Haiss, F., Sydekum, E., Schneider, R., Gullo, M., Wyss, M.T., Mueggler, T., Baltes, C., Rudin, M., Weber, B., Schwab, M.E., 2010. Rewiring of hindlimb corticospinal neurons after spinal cord injury. Nat. Neurosci. 13, 97–104.

Gonzalez-Lara, L.E., Xu, X., Hofstetrova, K., Pniak, A., Brown, A., Foster, P.J., 2009. In vivo magnetic resonance imaging of spinal cord injury in the mouse. J. Neurotrauma 26, 753–762.

Gonzalez-Lara, L.E., Xu, X., Hofstetrova, K., Pniak, A., Chen, Y., McFadden, C.D., Martinez-Santiesteban, F.M., Rutt, B.K., Brown, A., Foster, P.J., 2011. The use of cellular magnetic resonance imaging to track the fate of iron-labeled multipotent stromal cells after direct transplantation in a mouse model of spinal cord injury. Mol. Imag. Biol. 13, 702–711.

Goodman, J.W., 1976. Some fundamental properties of speckle. J. Opt. Soc. Am. 66, 1145.

Guzman, R., Uchida, N., Bliss, T.M., He, D., Christopherson, K.K., Stellwagen, D., Capela, A., Greve, J., Malenka, R.C., Moseley, M.E., Palmer, T.D., Steinberg, G.K., 2007. Long-term monitoring of transplanted human neural stem cells in developmental and pathological contexts with MRI. Proc. Natl. Acad. Sci. U.S.A. 104, 10211–10216.

Hecht, N., Woitzik, J., Dreier, J.P., Vajkoczy, P., 2009. Intraoperative monitoring of cerebral blood flow by laser speckle contrast analysis. Neurosurg. Focus 27, 1–6.

Helmchen, F., Denk, W., 2005. Deep tissue two-photon microscopy. Nat. Methods 2, 932–940.

Horiuchi, H., Oshima, Y., Ogata, T., Morino, T., Matsuda, S., Miura, H., Imamura, T., 2015. Evaluation of injured axons using two-photon excited fluorescence microscopy after spinal cord contusion injury in YFP-H line mice. Int. J. Mol. Sci. 16, 15785–15799.

Hu, S.L., Lu, P.G., Zhang, L.J., Li, F., Chen, Z., Wu, N., Meng, H., Lin, J.K., Feng, H., 2012a. In Vivo magnetic resonance imaging tracking of SPIO-labeled human umbilical cord mesenchymal stem cells. J. Cell. Biochem. 113, 1005–1012.

Hu, J., zhong, Wu, ding, T., Zhang, T., Zhao, Y. fang, Pang, J., Lu, H. bin, 2012b. Three-dimensional alteration of microvasculature in a rat model of traumatic spinal cord injury. J. Neurosci. Methods 204, 150–158.

Hu, C.-R., Zhang, D., Slipchenko, M.N., Cheng, J.-X., Hu, B., 2014. Label-free real-time imaging of myelination in the Xenopus laevis tadpole by in vivo stimulated Raman scattering microscopy. J. Biomed. Opt. 19, 086005.

Hu, J., Cao, Y., Wu, T., Li, D., Lu, H., 2015. 3D angioarchitecture changes after spinal cord injury in rats using synchrotron radiation phase-contrast tomography. Spinal Cord 53, 585–590.

Huang, L., Lin, X., Tang, Y., Yang, R., Li, A.H., Ye, J.C., Chen, K., Wang, P., Shen, H.Y., 2013. Quantitative assessment of spinal cord perfusion by using contrast-enhanced ultrasound in a porcine model with acute spinal cord contusion. Spinal Cord 51, 196–201.

Huang, J.H., Xu, Y., Yin, X.M., Lin, F.Y., 2020. Exosomes derived from miR-126-modified MSCs promote angiogenesis and neurogenesis and attenuate apoptosis after spinal cord injury in rats. Neuroscience 424, 133–145.

Jeon, M., Kim, J., Kim, C., 2016. Multiplane spectroscopic whole-body photoacoustic imaging of small animals in vivo. Med. Biol. Eng. Comput. 54, 283–294.

Johannssen, H.C., Helmchen, F., 2013. Two-photon imaging of spinal cord cellular networks. Exp. Neurol. 242, 18–26.
Jones, C.F., Cripton, P.A., Kwon, B.K., 2012. Gross morphological changes of the spinal cord immediately after surgical decompression in a large animal model of traumatic spinal cord injury. Spine (Phila. Pa. 1976) 37.
Joshi, M., Fehlings, M.G., 2002. Development and characterization of a novel, graded model of clip compressive spinal cord injury in the mouse: Part 1. Clip design, behavioral outcomes, and histopathology. J. Neurotrauma 19, 175–190.
Joshi, B., Duan, X., Kwon, R., Piraka, C., Elmunzer, B., Lu, S., Rabinsky, E., Beer, D., Appelman, H., Owens, S., Kuick, R., Doguchi, N., Turgeon, D., Wang, T., 2016. Multimodal endoscope can quantify wide-field fluorescence detection of Barrett's neoplasia. Endoscopy 48.
Kantelhardt, S.R., Kalasauskas, D., König, K., Kim, E., Weinigel, M., Uchugonova, A., Giese, A., 2016. In vivo multiphoton tomography and fluorescence lifetime imaging of human brain tumor tissue. J. Neurooncol. 127, 473–482.
Kawakami, N., 2018. Intravital imaging of T cells within the spinal cord. Intravital Imag. Dyn. Bone Immune Syst. Methods Protoc. 1763.
Kerschensteiner, M., Schwab, M.E., Lichtman, J.W., Misgeld, T., 2005. In vivo imaging of axonal degeneration and regeneration in the injured spinal cord. Nat. Med. 11, 572–577.
Khaing, Z.Z., Cates, L.N., DeWees, D.M., Hannah, A., Mourad, P., Bruce, M., Hofstetter, C.P., 2018. Contrast-enhanced ultrasound to visualize hemodynamic changes after rodent spinal cord injury. J. Neurosurg. Spine 29, 306–313.
Khaing, Z.Z., Cates, L.N., Hyde, J., DeWees, D.M., Hammond, R., Bruce, M., Hofstetter, C.P., 2020. Contrast-enhanced ultrasound for assessment of local hemodynamic changes following a rodent contusion spinal cord injury. Mil. Med. 7, 470–475.
Krishnan, V.S., Shin, S.S., Belegu, V., Celnik, P., Reimers, M., Smith, K.R., Pelled, G., 2019. Multimodal evaluation of TMS - induced somatosensory plasticity and behavioral recovery in rats with contusion spinal cord injury. Front. Neurosci. 13, 1–9.
Laskowski, C.J., Bradke, F., 2013. In vivo imaging: a dynamic imaging approach to study spinal cord regeneration. Exp. Neurol. 242, 11–17.
Lee, J., Satkunendrarajah, K., Fehlings, M.G., 2012. Development and characterization of a novel rat model of cervical spondylotic myelopathy: the impact of chronic cord compression on clinical, neuroanatomical, and neurophysiological outcomes. J. Neurotrauma 29, 1012–1027.
Lesage, F., Brieu, N., Dubeau, S., Beaumont, E., 2009. Optical imaging of vascular and metabolic responses in the lumbar spinal cord after T10 transection in rats. Neurosci. Lett. 454, 105–109.
Li, X., Li, H., He, X., Chen, T., Xia, X., Yang, C., Zheng, W., 2018. Spectrum- and time-resolved endogenous multiphoton signals reveal quantitative differentiation of premalignant and malignant gastric mucosa. Biomed. Opt Express 9, 453.
Liao, C.X., Wang, Z.Y., Zhou, Y., Zhou, L.Q., Zhu, X.Q., Liu, W.G., Chen, J.X., 2017. Label-free identification of the microstructure of rat spinal cords based on nonlinear optical microscopy. J. Microsc. 267, 143–149.
Luke, G.P., Yeager, D., Emelianov, S.Y., 2012. Biomedical applications of photoacoustic imaging with exogenous contrast agents. Ann. Biomed. Eng. 40, 422–437.
Luo, W., Li, P., Chen, S., Zeng, S., Luo, Q., 2007. Differentiating hemodynamic responses in rat primary somatosensory cortex during non-noxious and noxious electrical stimulation by optical imaging. Brain Res. 1133, 67–77.
Mai, C., Verleden, S.E., McDonough, J.E., Willems, S., De Wever, W., Coolen, J., Dubbeldam, A., Van Raemdonck, D.E., Verbeken, E.K., Verleden, G.M., Hogg, J.C., Vanaudenaerde, B.M., Wuyts, W.A., Verschakelen, J.A., 2017. Thin-section CT features of idiopathic pulmonary fibrosis correlated with micro-CT and histologic analysis. Radiology 283, 252.
Majdan, M., Plancikova, D., Nemcovska, E., Krajcovicova, L., Brazinova, A., Rusnak, M., 2017. Mortality due to traumatic spinal cord injuries in Europe: a cross-sectional and pooled analysis of population-wide data from 22 countries. Scand. J. Trauma Resuscitation Emerg. Med. 25.
Malisza, K.L., Stroman, P.W., 2002. Functional imaging of the rat cervical spinal cord. J. Magn. Reson. Imag. 16, 553–558.
Mallidi, S., Luke, G., Emelianov, S., 2011. Photoacoustic imaging in cancer detection, diagnosis, and treatment guidance. Trends Biotechnol. 29, 213–221.
Matsubayashi, K., Nagoshi, N., Komaki, Y., Kojima, K., Shinozaki, M., Tsuji, O., Iwanami, A., Ishihara, R., Takata, N., Matsumoto, M., Mimura, M., Okano, H., Nakamura, M., 2018. Assessing cortical plasticity after spinal cord injury by using resting-state functional magnetic resonance imaging in awake adult mice. Sci. Rep. 8, 1–8.
Misgeld, T., Nikic, I., Kerschensteiner, M., 2007. In vivo imaging of single axons in the mouse spinal cord. Nat. Protoc. 2, 263–268.
Monje, M., 2021. Spinal cord injury — healing from within. N. Engl. J. Med. 384, 182–184.
Moonen, G., Satkunendrarajah, K., Wilcox, J.T., Badner, A., Mothe, A., Foltz, W., Fehlings, M.G., Tator, C.H., 2016. A new acute impact-compression lumbar spinal cord injury model in the rodent. J. Neurotrauma 33, 278–289.
Murari, K., Li, N., Rege, A., Jia, X., All, A., Thakor, N., 2007. Contrast-enhanced imaging of cerebral vasculature with laser speckle. Appl. Opt. 46, 5340–5346.
Najafzadeh, E., Ghadiri, H., Alimohamadi, M., Farnia, P., Mehrmohammadi, M., Ahmadian, A., 2020. Evaluation of multi-wavelengths LED-based photoacoustic imaging for maximum safe resection of glioma: a proof of concept study. Int. J. Comput. Assist. Radiol. Surg. 15, 1053–1062.
Ogawa, S., Lee, T., Kay, A., Tank, D., 1990. Brain magnetic resonance imaging with contrast dependent on blood oxygenation. Proc. Natl. Acad. Sci. Unit. States Am. 87, 9868–9872.
Orem, B.C., Partain, S.B., Stirling, D.P., 2020a. Inhibiting store-operated calcium entry attenuates white matter secondary degeneration following. SCI. Neurobiol. Dis. 136.
Orem, B.C., Rajaee, A., Stirling, D.P., 2020b. IP3R-mediated intra-axonal Ca2+ release contributes to secondary axonal degeneration following contusive spinal cord injury. Neurobiol. Dis. 146.
Oshima, Y., Horiuch, H., Honkura, N., Hikita, A., Ogata, T., Miura, H., Imamura, T., 2014. Intravital multiphoton fluorescence imaging and optical manipulation of spinal cord in mice, using a compact fiber laser system. Laser Surg. Med. 46, 563–572.
Otzel, D.M., Conover, C.F., Ye, F., Phillips, E.G., Bassett, T., Wnek, R.D., Flores, M., Catter, A., Ghosh, P., Balaez, A., Petusevsky, J., Chen, C., Gao, Y., Zhang, Y., Jiron, J.M., Bose, P.K., Borst, S.E., Wronski, T.J., Aguirre, J.I., Yarrow, J.F., 2019. Longitudinal examination of bone loss in male rats after moderate–severe contusion spinal cord injury. Calcif. Tissue Int. 104, 79–91.
Patel, C.B., Cohen, D.M., Ahobila-Vajjula, P., Sundberg, L.M., Chacko, T., Narayana, P.A., 2009. Effect of VEGF treatment on the blood-spinal cord barrier permeability in experimental spinal cord injury: dynamic contrast-enhanced magnetic resonance imaging. J. Neurotrauma 26, 1005–1016.
Patel, S.P., Smith, T.D., Vanrooyen, J.L., Powell, D., Cox, D.H., Sullivan, P.G., Rabchevsky, A.G., 2016. Serial diffusion tensor imaging in vivo predicts long-term functional recovery and histopathology in rats following different severities of spinal cord injury. J. Neurotrauma 33, 917–928.
Ramu, J., Bockhorst, K.H., Mogatadakala, Kishore V., Narayana, P.A., 2006. Functional magnetic resonance imaging in rodents: methodology and application to spinal cord injury. J. Neurosci. Res. 84, 1235–1244.
Richards, L.M., Kazmi, S.S., Olin, K.E., Waldron, J.S., Fox, D.J., Dunn, A.K., 2017. Intraoperative multi-exposure speckle imaging of cerebral blood flow. J. Cerebr. Blood Flow Metabol. 37, 3097–3109.
Sanderson, M., Smith, I., Parker, I., Bootman, M., 2014. Fluorescence microscopy. Cold Spring Harb. Protoc. 10.
Schilling, K.G., Nath, V., Hansen, C., Parvathaneni, P., Blaber, J., Gao, Y., Neher, P., Aydogan, D.B., Shi, Y., Ocampo-Pineda, M., Schiavi, S., Daducci, A., Girard, G., Barakovic, M., Rafael-Patino, J., Romascano, D., Rensonnet, G., Pizzolato, M., Bates, A., Fischi, E., Thiran, J.P., Canales-Rodríguez, E.J., Huang, C., Zhu, H., Zhong, L., Cabeen, R., Toga, A.W., Rheault, F., Theaud, G., Houde, J.C., Sidhu, J., Chamberland, M., Westin, C.F., Dyrby, T.B., Verma, R., Rathi, Y., Irfanoglu, M.O., Thomas, C., Pierpaoli, C., Descoteaux, M., Anderson, A.W., Landman, B.A., 2019. Limits to anatomical accuracy of diffusion tractography using modern approaches. Neuroimage 185, 1–11.
Schwartz, E.D., Hackney, D.B., 2003. Diffusion-weighted MRI and the evaluation of spinal cord axonal integrity following injury and treatment. Exp. Neurol. 184, 570–589.
Senarathna, J., Rege, A., Li, N., Thakor, N.V., 2013. Laser speckle contrast imaging: theory, instrumentation and applications. IEEE Rev. Biomed. Eng. 6, 99–110.
Sensarn, S., Zavaleta, C.L., Segal, E., Rogalla, S., Lee, W., Gambhir, S.S., Bogyo, M., Contag, C.H., 2016. A clinical wide-field fluorescence endoscopic device for molecular imaging demonstrating cathepsin protease activity in colon cancer. Mol. Imag. Biol. 18, 820–829.
Shen, J., Zhong, X.-M., Duan, X.-H., Cheng, L.-N., Hong, G., Bi, X.-B., Liu, Y., 2009. Magnetic resonance imaging of mesenchymal stem cells labeled with dual (MR and fluorescence) agents in rat spinal cord injury. Acad. Radiol. 16, 1142–1154.
Shi, R., Jin, C., Xie, H., Zhang, Y., Li, X., Dai, Q., Kong, L., 2019. Multi-plane, wide-field fluorescent microscopy for biodynamic imaging in vivo. Biomed. Opt Express 10, 6625.
Singh, A., Tetreault, L., Kalsi-Ryan, S., Nouri, A., Fehlings, M.G., 2014. Global prevalence and incidence of traumatic spinal cord injury. Clin. Epidemiol. 6, 309–331.
Skuba, A., Himes, B.T., Son, Y., 2011. Live Imaging of Dorsal Root Axons after Rhizotomy. Jove.
Soares, J.M., Marques, P., Alves, V., Sousa, N., 2013. A hitchhiker's guide to diffusion tensor imaging. Front. Neurosci. 7, 1–14.
Song, W., Song, G., Zhao, C., Li, X., Pei, X., Zhao, W., Gao, Y., Rao, J.S., Duan, H., Yang, Z., 2018. Testing pathological variation of white matter tract in adult rats after severe spinal cord injury with MRI. BioMed Res. Int. 2018.
Soubeyrand, M., Laemmel, E., Dubory, A., Vicaut, E., Court, C., Duranteau, J., 2012. Real-time and spatial quantification using contrast-enhanced ultrasonography of spinal cord perfusion during experimental spinal cord injury. Spine (Phila. Pa. 1976) 37.
Soubeyrand, M., Badner, A., Vawda, R., Chung, Y.S., Fehlings, M.G., 2014a. Very high resolution ultrasound imaging for real-time quantitative visualization of vascular disruption after spinal cord injury. J. Neurotrauma 31, 1767–1775.
Soubeyrand, M., Badner, A., Vawda, R., Chung, Y.S., Fehlings, M.G., 2014b. Very high resolution ultrasound imaging for real-time quantitative visualization of vascular disruption after spinal cord injury. J. Neurotrauma 31, 1767–1775.
Soubeyrand, M., Dubory, A., Laemmel, E., Court, C., Vicaut, E., Duranteau, J., 2014c. Effect of norepinephrine on spinal cord blood flow and parenchymal hemorrhage size in acute-phase experimental spinal cord injury. Eur. Spine J. 23, 658–665.
Strotton, M.C., Bodey, A.J., Wanelik, K., Hobbs, C., Rau, C., Bradbury, E.J., 2021. The spatiotemporal spread of cervical spinal cord contusion injury pathology revealed by 3D in-line phase contrast synchrotron X-ray microtomography. Exp. Neurol. 336.
Sundberg, L.M., Herrera, J.J., Narayana, P.A., 2010. In vivo longitudinal MRI and behavioral studies in experimental spinal cord injury. J. Neurotrauma 27, 1753–1767.
Sundberg, L.M., Herrera, J.J., Narayana, P.A., 2011. Effect of vascular endothelial growth factor treatment in experimental traumatic spinal cord injury: in vivo longitudinal assessment. J. Neurotrauma 28, 565–578.
Tang, P., Zhang, Y., Chen, C., Ji, X., Ju, F., Liu, X., Gan, W.B., He, Z., Zhang, S., Li, W., Zhang, L., 2015. In vivo two-photon imaging of axonal dieback, blood flow, and calcium influx with methylprednisolone therapy after spinal cord injury. Sci. Rep. 5, 1–10.
Tang, P., Zhang, Y., Chen, C., Xinran, J., Ju, F., Liu, X., Gan, W.-B., He, Z., Zhang, S., Li, W., Zhang, L., and Kirby, F.M. ([date unknown]). In Vivo Two-Photon Imaging of

Axonal Dieback, Blood Flow, and Calcium Influx with Methylprednisolone Therapy after Spinal Cord Injury.
Tator, C.H., 1991. Review of experimental spinal cord injury with emphasis on the local and systemic circulatory effects. Neurochirurgie 37, 291–302.
Theer, P., Hasan, M.T., Denk, W., 2003. Two-photon imaging to a depth of 1000 μm in living brains by use of a Ti:Al_2O_3 regenerative amplifier. Opt. Lett. 28, 1022.
Tschuchnig, M.E., Zillner, D., Romanelli, P., Hercher, D., Heimel, P., Oostingh, G.J., Couillard-Després, S., Gadermayr, M., 2021. Quantification of anomalies in rats' spinal cords using autoencoders. Comput. Biol. Med. 138.
Tu, T., Kim, J., Wang, J., Song, S., 2010. Full tensor diffusion imaging is not required to assess the white-matter integrity in mouse contusion in mouse contusion spinal cord injury. J. Neurotrauma 262, 253–262.
Tu, T.-W., Kim, J.H., Yin, F.Q., Jakeman, L.B., Song, S.-K., 2013. The impact of myelination on axon sparing and locomotor function recovery in spinal cord injury assessed using diffusion tensor imaging. NMR Biomed. 26, 1484–1495.
Uckermann, O., Galli, R., Beiermeister, R., Sitoci-Ficici, K.H., Later, R., Leipnitz, E., Neuwirth, A., Chavakis, T., Koch, E., Schackert, G., Steiner, G., Kirsch, M., 2015. Endogenous two-photon excited fluorescence provides label-free visualization of the inflammatory response in the rodent spinal cord. Biomed Res. Int. 2015.
Uhl, C., Markel, M., Broggini, T., Nieminen, M., Kremenetskaia, I., Vajkoczy, P., Czabanka, M., 2018. EphB4 mediates resistance to antiangiogenic therapy in experimental glioma. Angiogenesis 21, 873–881.
Vajkoczy, P., Goldbrunner, R., Farhadi, M., Vince, G., Schilling, L., Tonn, J.C., Schmiedek, P., Menger, M.D., 1999. Glioma cell migration is associated with glioma-induced angiogenesis in vivo. Int. J. Dev. Neurosci. 17, 557–563.
Vajkoczy, P., Laschinger, M., Engelhardt, B., 2001. Alpha4-integrin-VCAM-1 binding mediates G protein-independent capture of encephalitogenic T cell blasts to CNS white matter microvessels. J. Clin. Invest. 108, 557–565.
Vawda, R., Badner, A., Hong, J., Mikhail, M., Lakhani, A., Dragas, R., Xhima, K., Barretto, T., Librach, C.L., Fehlings, M.G., 2019. Early intravenous infusion of mesenchymal stromal cells exerts a tissue source age-dependent beneficial effect on neurovascular integrity and neurobehavioral recovery after traumatic cervical spinal cord injury. Stem Cells Transl. Med. 8, 639–649.
Volz, K.R., Evans, K.D., Kanner, C.D., Michele Basso, D., 2016. Exploring targeted contrast-enhanced ultrasound to detect neural inflammation: an example of standard nomenclature. J. Diagn. Med. Sonogr. 32, 313–323.
Volz, K.R., Evans, K.D., Kanner, C.D., Buford, J.A., Freimer, M., Sommerich, C.M., 2017. Molecular ultrasound imaging of the spinal cord for the detection of acute inflammation. J. Diagn. Med. Sonogr. 33, 454–463.
Wang, L., Shi, Q., Dai, J., Gu, Y., Feng, Y., Chen, L., 2017. Increased vascularization promotes functional recovery in the transected spinal cord rats by implanted vascular endothelial growth factor-targeting collagen scaffold. J. Orthop. Res. 36, 1024–1034.
Werndle, M.C., Saadoun, S., Phang, I., Czosnyka, M., Varsos, G.V., Czosnyka, Z.H., Smielewski, P., Jamous, A., Anthony Bell, B., Zoumprouli, A., Papadopoulos, M.C., 2014. Monitoring of spinal cord perfusion pressure in acute spinal cord injury: initial findings of the injured spinal cord pressure evaluation study. Crit. Care Med. 42.
Wilkins, N., Skinner, N.P., Motovylyak, A., Schmit, B.D., Kurpad, S., Budde, M.D., 2020. Evolution of magnetic resonance imaging as predictors and correlates of functional outcome after spinal cord contusion injury in the rat. J. Neurotrauma 37, 889–898.
Woitzik, J., Hecht, N., Pinczolits, A., Sandow, N., Major, S., Winkler, M.K.L., Weber-Carstens, S., Dohmen, C., Graf, R., Strong, A.J., Dreier, J.P., Vajkoczy, P., 2013. Propagation of cortical spreading depolarization in the human cortex after malignant stroke. Neurology 80, 1095–1102.
Wu, X., Xu, X., Liu, Q., Ding, J., Liu, J., Huang, Z., Huang, Z., Wu, X., Li, R., Yang, Z., Jiang, H., Liu, J., Zhu, Q., 2021. Unilateral cervical spinal cord injury induces bone loss and metabolic changes in non-human primates (Macaca fascicularis). J. Orthop. Transl. 29, 113–122.
Xu, M., Wang, L.V., 2006. Photoacoustic imaging in biomedicine. Rev. Sci. Instrum. 77.
Xu, Z.-X., Zhang, L.-Q., Wang, C.-S., Chen, R.-S., Li, G.-S., Guo, Y., Xu, W.-H., 2017. Acellular spinal cord scaffold implantation promotes vascular remodeling with sustained delivery of VEGF in a rat spinal cord hemisection model. Curr. Neurovascular Res. 14.
Yahyapour, R., Farhood, B., Graily, G., Rezaeyan, A., Rezapoor, S., Abdollahi, H., Cheki, M., Amini, P., Fallah, H., Najafi, M., Motevaseli, E., 2018. Stem cell tracing through MR molecular imaging. Tissue Eng. Regen. Med. 15, 249–261.
Yang, Z., Xie, W., Ju, F., khan, A., Zhang, S., 2017a. In vivo two-photon imaging reveals a role of progesterone in reducing axonal dieback after spinal cord injury in mice. Neuropharmacology 116, 30–37.
Yang, Z., Xie, W., Ju, F., Khan, A., Zhang, S., 2017b. In vivo two-photon imaging reveals a role of progesterone in reducing axonal dieback after spinal cord injury in mice. Neuropharmacology 116, 30–37.
Yarrow, J.F., Conover, C.F., Beggs, L.A., Beck, D.T., Otzel, D.M., Balaez, A., Combs, S.M., Miller, J.R., Ye, F., Aguirre, J.I., Neuville, K.G., Williams, A.A., Conrad, B.P., Gregory, C.M., Wronski, T.J., Bose, P.K., Borst, S.E., 2014. Testosterone dose dependently prevents bone and muscle loss in rodents after spinal cord injury. J. Neurotrauma 31, 834–845.
Zambrano-Rodríguez, P.C., Bolaños-Puchet, S., Reyes-Alva, H.J., García-Orozco, L.E., Romero-Piña, M.E., Martinez-Cruz, A., Guízar-Sahagún, G., Medina, L.A., 2019. Micro-CT myelography using contrast-enhanced digital subtraction: feasibility and initial results in healthy rats. Neuroradiology 61, 323–330.
Zambrano-Rodríguez, P.C., Bolaños-Puchet, S., Reyes-Alva, H.J., de Los Santos, R.A., Martinez-Cruz, A., Guízar-Sahagún, G., Medina, L.A., 2021a. High-resolution micro-CT myelography to assess spinal subarachnoid Space changes after spinal cord injury in rats. J. Neuroimaging 31, 79–89.
Zambrano-Rodríguez, P.C., Bolaños-Puchet, S., Reyes-Alva, H.J., de Los Santos, R.A., Martinez-Cruz, A., Guízar-Sahagún, G., Medina, L.A., 2021b. High-resolution micro-CT myelography to assess spinal subarachnoid Space changes after spinal cord injury in rats. J. Neuroimaging 31, 79–89.
Zhang, Y., Zhang, L., Shen, J., Chen, C., Mao, Z., Li, W., Gan, W.-B., Tang, P., 2014. Two-photon-Excited fluorescence microscopy as a tool to investigate the efficacy of methylprednisolone in a mouse spinal cord injury model. Spine (Phila. Pa. 1976 39, E493–E499.
Zhang, Y., Zhang, L., Ji, X., Pang, M., Ju, F., Zhang, J., Li, W., Zhang, S., He, Z., Gan, W.-B., Tang, P., 2015. Two-photon microscopy as a tool to investigate the therapeutic time window of methylprednisolone in a mouse spinal cord injury model. Restor. Neurol. Neurosci. 33, 291–300.